Dynamic characterization of external and internal mass transport in heterotrophic biofilms from microsensors measurements

Xavier Guimerà[1], Antonio David Dorado[1*], Anna Bonsfills[1], Gemma Gabriel[2,3], David Gabriel[4], Xavier Gamisans[1]

[1]*Department of Mining Engineering and atural Resources, Universitat Politècnica de Catalunya, Avinguda de les Bases de Manresa 61-73, 08240 Manresa, Spain*

[2]*Instituto de Microelectrónica de Barcelona, IMB-CNM (CSIC), Esfera UAB, Campus Universitat Autònoma de Barcelona, 08193 Bellaterra, Barcelona, Spain*

[3]*Biomedical Research Networking Center in Bioengineering, Biomaterials and Nanomedicine (CIBER-BBN), Zaragoza, Spain*

[4]*Department of Chemical Engineering, Universitat Autònoma de Barcelona, Edifici Q, 08193 Bellaterra, Barcelona, Spain*

* Corresponding author. Tel.: +34 938 777 230, E-mail: toni.dorado@upc.edu

E-mail addresses: xavier.guimera@emrn.upc.edu (X. Guimerà), toni.dorado@upc.edu (A. D. Dorado), annab@emrn.upc.edu (A. Bonsfills), gemma.gabriel@imb-cnm.csic.es (G. Gabriel), david.gabriel@uab.cat (D. Gabriel), xavierg@emrn.upc.edu (X. Gamisans).

Abstract

Knowledge of mass transport mechanisms in biofilm-based technologies such as biofilters is essential to improve bioreactors performance by preventing mass transport limitation. External and internal mass transport in biofilms was characterized in heterotrophic biofilms grown on a flat plate bioreactor. Mass transport resistance through the liquid-biofilm interphase and diffusion within biofilms were quantified by in situ measurements using microsensors with a high spatial resolution (<50 μm). Experimental conditions were selected using a mathematical procedure based on the Fisher Information Matrix to increase the reliability of experimental data

and minimize confidence intervals of estimated mass transport coefficients. The sensitivity of external and internal mass transport resistances to flow conditions within the range of typical fluid velocities over biofilms (Reynolds numbers between 0.5 and 7) was assessed. Estimated external mass transfer coefficients at different liquid phase flow velocities showed discrepancies with studies considering laminar conditions in the diffusive boundary layer near the liquid-biofilm interphase. The correlation of effective diffusivity with flow velocities showed that the heterogeneous structure of biofilms defines the transport mechanisms inside biofilms. Internal mass transport was driven by diffusion through cell clusters and aggregates at Re below 2.8. Conversely, mass transport was driven by advection within pores, voids and water channels at Re above 5.6. Between both flow velocities, mass transport occurred by a combination of advection and diffusion. Effective diffusivities estimated at different biofilm densities showed a linear increase of mass transport resistance due to a porosity decrease up to biofilm densities of 50 g VSS·L^{-1}. Mass transport was strongly limited at higher biofilm densities. Internal mass transport results were used to propose an empirical correlation to assess the effective diffusivity within biofilms considering the influence of hydrodynamics and biofilm density.

Keywords: dissolved oxygen microsensors, biofilm profiling, mass transfer resistance, effective diffusivity, mass transport modelling.

Nomenclature

a	specific mass transfer area ($m^2 \cdot m^{-3}$)
$A_{transfer}$	interfacial area of the monitored system (m^2)
$C_{DO,b}$	DO concentration inside the biofilm ($mg \cdot L^{-1}$)
$C_{DO,B}$	DO concentration on biofilm surface ($mg \cdot L^{-1}$)
$C_{DO,B\ (t=0)}$	initial DO concentration on biofilm surface ($mg \cdot L^{-1}$)
$C_{DO,L}$	DO concentration inside the liquid boundary layer ($mg \cdot L^{-1}$)
$C_{DO,L\ (i)}$	DO concentration in the liquid phase at the inlet of a FPB section ($mg \cdot L^{-1}$)
$C_{DO,L\ (inlet)}$	DO concentration in the liquid phase at the inlet of the FPB ($mg \cdot L^{-1}$)
$C_{DO,L\ (o)}$	DO concentration in the liquid phase at the outlet of a FPB section ($mg \cdot L^{-1}$)

$C_{DO,L\ (t=0)}$	initial DO concentration in the liquid boundary layer ($mg \cdot L^{-1}$)
D_b	effective diffusivity within biofilms ($m^2 \cdot s^{-1}$)
D_i	the effective diffusivity within the boundary layer ($m^2 \cdot s^{-1}$)
D_r	dimensionless effective diffusivity (-)
F	objective function in optimization procedure for parameters estimation
k_L	external mass transfer coefficient ($m \cdot s^{-1}$)
L_c	boundary layer thickness (m)
n	number of experimental measurements
Q_L	liquid flow rate ($m^3 \cdot s^{-1}$)
Re	Reynolds number
Sc	Schmidt number
Sh	Sherwood number
t	time (s)
t_{exp}	monitoring time (s)
V_L	liquid phase volume (m)
$v_{sampling}$	sampling frequency (s^{-1})
X_b	biofilm density (g VSS$\cdot L^{-1}$)
$y_{\theta,i}$	simulated oxygen concentration in optimization procedure ($mg \cdot L^{-1}$)
$y_{exp,I}$	experimentally measured oxygen concentration in optimization procedure ($mg \cdot L^{-1}$)
z	biofilm depth (m)
$z_{profile}$	depth of DO profile (μm)
$\Delta z_{profile}$	distance between monitoring points (μm)

1. Introduction

Biofilters and biotrickling filters are the most important biofilm-based reactors for air pollution control. However, the limited knowledge about biofilms performance due to large technical limitations in biofilms monitoring, mainly due to their reduced size (ranging from few microns to few millimeters), has led to often assume large model simplifications in biofiltration

81 modeling (Beyenal and Lewandowski, 2005). Characterization of mass transport and biological
82 reactions within biofilms is essential to improve biofilms models and therefore, our ability to
83 design and operate biofilm reactors.

84 Two main phenomena are considered when modeling biofilms performance (Bishop et al.,
85 1995; C. Picioreanu et al., 2000): (1) pollutants and substrates transport at the liquid-biofilm
86 interphase (external mass transport) and within biofilms (internal mass transport) and (2) the
87 biodegradation of pollutants in the biofilm. Literature is abundant in assessing biokinetic
88 parameters, which are usually adapted from suspended cultures studies for further biofilm
89 modeling (Bonilla-Blancas et al., 2015; Hille et al., 2009; Mannucci et al., 2012) despite this
90 approach is somehow questionable due to physiological differences between attached and
91 suspended growth systems (Yurt et al., 2003). Oppositely, literature is scarce in the
92 characterization of external and internal mass transport in biofilm modelling. External mass
93 transport resistance is often modeled through mass transfer coefficients (Horn and Hempel,
94 1997) usually calculated as a function of hydrodynamic conditions in the reactor (Piccioreanu et
95 al. 2000). Different works have studied external mass transport resistance in the liquid boundary
96 layer from experimental measurements with microsensors (Horn and Hempel, 1995; Wäsche et
97 al., 2002; Zhang and Bishop, 1995). However, these measurements only provided limited
98 information of external mass transport resistance since did not considered diffusive and
99 convective phenomena within the boundary layer as suggested by different authors (Beyenal
100 and Lewandowski, 2000; Wäsche et al., 2002). On the other hand, internal mass transport in
101 biofilm systems is commonly addressed by diffusive mechanisms following Fick's law
102 (Stewart, 2003).

103 Effective diffusivities within biofilms are highly influenced by biofilms structure and
104 heterogeneity. Some works have considered the effect of biofilms heterogeneity in effective
105 diffusivity correlations through the use of different structural macroscopic parameters such as
106 biofilm density, porosity and tortuosity. Although the use of these correlations for effective
107 diffusivity is sometimes used in biofiltration models, its reliability is under suspect. Most of

these researches were based on theoretical models (Zhang and Bishop, 1994) or important theoretical assumptions (Hinson and Kocher, 1996). Oppositely, several works have shown the high performance of microsensors measurements for the quantification of effective diffusivity within biofilms (Beuling et al., 1999; Fu et al., 1994; Hille et al., 2009; Ning et al., 2012). However, the reliability of these studies is compromised since empirical correlations for effective diffusivity estimation within biofilms were developed combining experimental estimates inside biofilms showing dry mass densities between 10 and 65 $g \cdot L^{-1}$, and sludge granules, with dry mass densities above 100 $g \cdot L^{-1}$.

The confidence intervals of mass transport parameters are not commonly determined. However, the assessment of confidence intervals is as important as the estimation of the parameter. A mathematical method based on the Fisher Information Matrix (FIM) is a proven procedure that accurately provides confidence intervals of estimated parameters. FIM method is based on the calculation of the covariance inverse matrix and is directly associated to the uncertainty of estimated parameters and the quality and quantity of experimental data. In addition, the FIM method can be adapted for optimal experiment design (Dochain and Vanrolleghem, 2001), thus the reliability of mass transport parameters can be enhanced due to the selection of optimal experimental conditions during the design of the experiments.

The goal of this work was to take advantage of the high resolution of microsensors measurements (10 μm) to experimentally quantify external and internal mass transport resistance. Oxygenation profiles were recorded using a dissolved oxygen (DO) microsensor specially designed for biofilms profiling (Moya et al., 2014). Oxygenation data were used to develop methodologies for mass transport parameters estimation to further investigate the influence of hydrodynamic conditions and biofilm density on external and internal mass transport. Reliability of estimated parameters was increased by selecting the optimal experimental conditions, evaluating the parameter sensitivities and the quality of estimated parameters (confidence intervals).

2. Materials and Methods

2.1 Development of an heterotrophic biofilm

Mass transport phenomena were studied in a heterotrophic biofilm grown in a flat plate bioreactor (FPB), shown in figure 1. The reactor consisted of an open channel, manufactured in methacrylate (PMMA), 20 cm in length, 3.5 cm in width, and 1.3 cm in depth. The wall effect in the open channel was assessed in modeling studies (Prades et al., 2015) concluding that this effect could be neglected in laminar flow conditions. The reactor setup included two tanks of 40 mL (depicted in figure 1), at the inlet and the outlet of the open channel, to control the thickness of the liquid film over the biofilm. The FPB was fed with the nutrient solution (mineral medium containing 13 $g \cdot L^{-1}$ of glucose as carbon source) using a peristaltic pump (MCP Standard, Ismatec, Germany). The liquid phase was recirculated through the reactor using a second peristaltic pump (Miniplus 3, Gilson, France). A mixing chamber was placed in the recirculation line to manually adjust the DO concentration in the liquid phase by bubbling air-N_2 mixtures. More details about reactor setup can be found in Guimerà et al. (2014)

The reactor was sterilized as described in Guimerà et al. (2014) and later seeded with 40 ml of a sludge obtained from a wastewater treatment pilot plant for biological phosphorous removal (Guerrero et al., 2011). The inoculated heterotrophic bacteria consortium, enriched with polyphosphate-accumulating bacteria, had a cells concentration of 4 $g \cdot L^{-1}$ of volatile suspended solids (VSS). The remaining volume (110 mL) was filled with mineral medium, which composition is detailed in Dorado et al. (2012). The reactor was operated in batch mode at a low recirculation velocity (2.5 $m \cdot h^{-1}$) for 24-48 hours to promote bacteria immobilization on the reactor plate. Then, reactor operation was switched to continuous mode until a steady biofilm thickness was visually observed, which occurred after around 10 days. The hydraulic residence time (defined by the ratio between liquid phase volume and feed flowrate) and the liquid phase velocity (defined by the ratio between recirculation flowrate and liquid phase section) were set at 8 h and 10 $m \cdot h^{-1}$ respectively, to reproduce typical growth conditions of biomass in biotrickling filters (Devinny et al., 1999). The reactor was kept at room temperature (between

161 20ºC and 25ºC) and without artificial illumination during biofilm growth and along the
162 experimental period.

163 The glucose content in the liquid phase was periodically measured along the reactor using a
164 refractometer (Refracto 30GS, Mettler-Toledo, Switzerland) to check that microbial growth was
165 not limited by the carbon source. The pH in the liquid phase was also measured and manually
166 adjusted to pH 7 by adding either 0.1 M HCl or NaOH solutions. The density profile observed
167 along the reactor length, was assessed by protein analysis (Bradford, 1976) of small biofilm
168 samples (0.1 ml). Protein analysis was selected for biofilm density measurement since it showed
169 a good correlation with VSS concentration (section S1 of the Supplementary Material).

170 Previous to effective diffusivity estimation experiments,, biofilm was deactivated by
171 recirculating a NaN_3 solution (0.2 $g \cdot L^{-1}$) during 1 hour in order to prevent biological activity
172 while maintaining diffusion features through biofilms (Horn and Morgenroth, 2006).

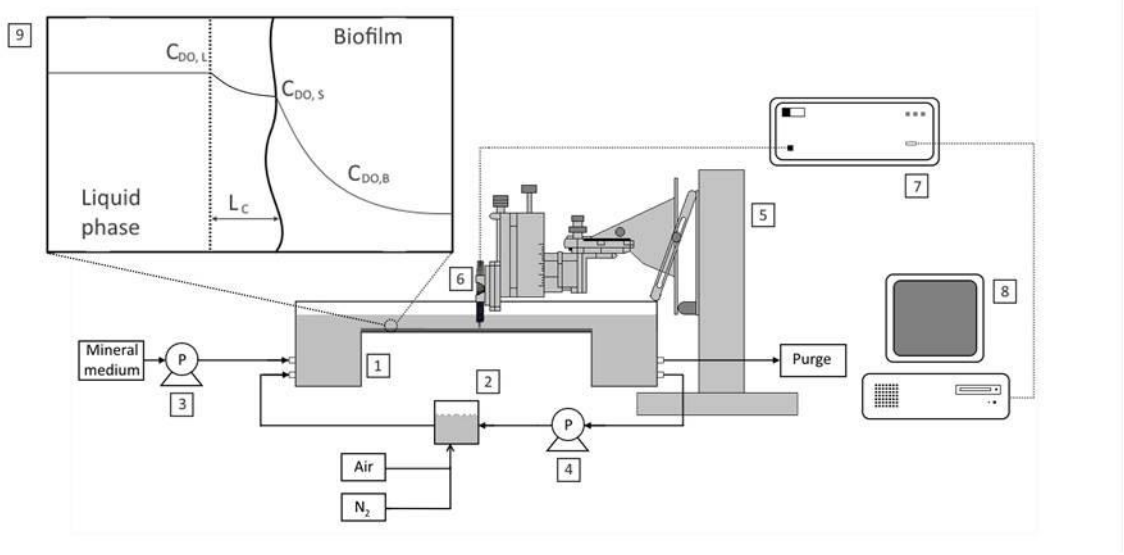

Figure 1. Schematic of the experimental setup: (1) FPB; (2) mixing chamber; (3) feeding pump; (4) recirculation pump; (5) micromanipulator; (6) microsensor; (7) microsensor amplifier; (8) data-acquisition system; (9) conceptual diagram of the liquid and biofilm phases (where $C_{DO,L}$ is DO concentration in the liquid phase; $C_{DO,S}$ is DO concentration at the biofilm surface; $C_{DO,B}$ is the DO concentration within the biofilm; and L_C is the thickness of the boundary layer).

173

174 **2.2 Experimental measurements**

175 *2.2.1 Microsensors*

External and internal mass transport were characterized in biofilms through different DO measurements using microsensors. DO measurements used in the quantification of external mass transfer resistance were performed with a commercial Clark-type microsensor (OXI-25, Unisense, Denmark). The microsensors, connected to a 4-channel amplifier (Microsensor Multimeter, Unisense, Denmark), were moved through a reactor section in 50 µm steps by means of a micromanipulator (MM33-2, Unisense, Denmark). DO profiles were recorded using a data acquisition software (Sensor Trace Basic, Unisense, Denmark). Two-point calibrations were performed prior to profiles recording.

On the other hand, effective diffusivities within biofilms were experimentally quantified from DO profiles recorded using a DO microsensor based on microfabrication technology as described elsewhere (Moya et al., 2014). This sensor consisted of an array of eleven gold-disk working electrodes and a rectangular gold counter electrode (CE), mounted on a minimally invasive microfabricated needle. Detailed information of design characteristics are detailed in section S2 of the Supplementary Material. The array of microelectrodes was designed to be inserted vertically inside a biofilm, allowing the simultaneous monitoring of DO concentration at different biofilm depths. The DO was monitored using an external reference electrode (RE) (REF321, Radiometer analytical, France). The electrodes were simultaneously calibrated before profile recordings using a two-point calibration procedure. Microelectrodes were polarized at an oxygen reduction potential of -850 mV using an 8-channel potentiostat (1010C, CH-Instruments, USA). Generated reduction currents were used to quantify the DO concentration.

2.2.2. Microsensors measurements

Mass transport resistances were estimated through deactivated biofilms grown in the FPB by assessing the evolution of the DO concentration in the liquid boundary layer, the biofilm surface and inside the biofilm. Mass transport resistances were estimated through deactivated biofilms grown in the FPB by assessing the evolution of the DO concentration in the liquid boundary layer, the biofilm surface and inside the biofilm. The depth within a biofilm section of the

boundary layer liquid side and of the biofilm surface were determined from a DO profile recorded from the liquid phase to the deeper part of the biofilm (figure 2). The DO microprofile was interpreted according to Wäsche et al., (2002). The linear section at the beginning of the recorded profile was assumed to belong to the completely mixed bulk phase. On the other side, the nearly vertical section of the profile belonged to the biofilm. The boundary layer is defined as the depth between both linear sections; the first point is defined as the liquid side boundary layer and the second one as the biofilm surface. The experimental procedure followed during oxygenation profiles recording is presented below.

First, the bioreactor was deoxygenated by bubbling N_2 in the mixing chamber. Once the desired DO concentration was reached, which was set according to the results of the experimental design, N_2 bubbling was switched to air sparging. DO was simultaneously monitored at the points of interest during the re-aeration phase. Experiments for external mass transport coefficients estimation were performed positioning two Clark-type microsensors in the boundary layer liquid side and on the biofilm surface and recording the DO evolution at these points during the re-aireation procedure. On the other hand, effective diffusivities were quantified inserting the microfabricated DO microsensor inside biofilms. An array of 8 microelectrodes (according to the data acquisition system capacity) was positioned from the biofilm surface inwards. Then, the evolution of the DO concentration at 8 different depths inside the biofilm, separated by 50 µm, was simultaneously recorded during the re-aireation procedure.

2.3. Biofilm modeling

External and internal mass transports through biofilms were modeled to quantify mass transport resistances using microsensors measurements.

2.3.1. External mass transport

Biofilms surface were assumed to be separated from the bulk liquid phase by a laminar layer in which external mass transfer resistance occurred. Therefore, film theory was applied to describe

the mass flux towards the interphase using an external mass transfer coefficient. Oxygen evolution in the liquid side of the boundary layer and on the biofilm surface, of a biofilm section, was modeled using an external mass transfer coefficient, as shown in equation (1) and equation (2) respectively.

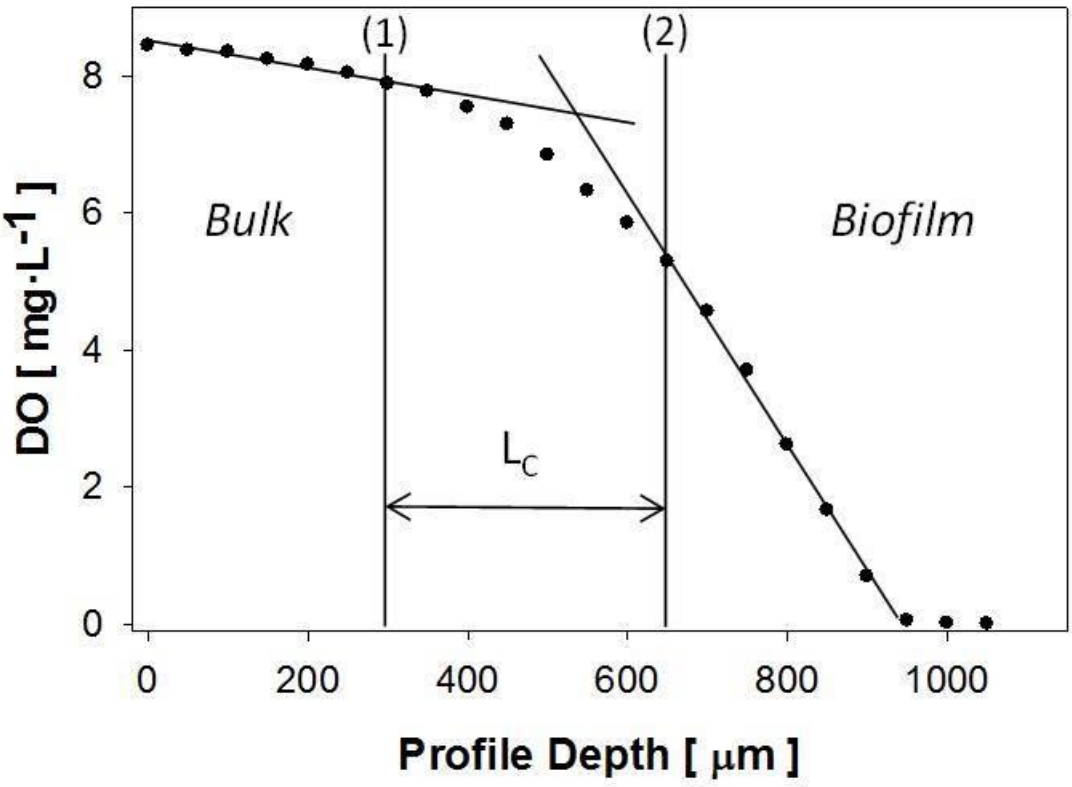

Figure 2. Analysis of an oxygen microprofile, used to define the boundary layer, and to locate the boundary layer liquid side (1) and the biofilm surface (2) at a biofilm section.

$$\frac{dC_{DO,L}}{dt} = \frac{1}{V_L} \cdot \left[Q_L \cdot \left(C_{DO,L(i)} - C_{DO,L(o)} \right) - k_L \cdot A_{transfer} \cdot \left(C_{DO,L} - C_{DO,B} \right) \right] \qquad (1)$$

$$\frac{dC_{DO,B}}{dt} = k_L \cdot a \cdot \left[C_{DO,L} - C_{DO,B} \right] \qquad (2)$$

Where C_{DO} is the DO concentration ($mg \cdot L^{-1}$), t is time (s), V_L is the volume of the liquid phase in a reactor section (m^3), Q_L is the liquid flowrate over biofilm ($m^3 \cdot s^{-1}$), k_L is the liquid side mass transfer coefficient across the boundary layer ($m \cdot s^{-1}$), $A_{transfer}$ is the transfer area of the reactor

section (m^2), a is the specific mass transfer area ($m^2 \cdot m^{-3}$), the subscripts L and B refer to the bulk liquid and biofilm surface, and subscripts *(i)* and *(o)* refer to the inlet and the outlet of the reactor section. Oxygen transfer across the liquid surface was neglected. This assumption was based on small oxygenation rates ($3.9 \cdot 10^{-2}$ $mg \cdot L^{-1} \cdot s^{-1} \cdot m^{-2}$) observed in preliminary studies (data not shown). The specific mass transfer area in a reactor section was defined as the ratio between biofilm transfer area (A_{trans}) and the volume (V_L) of the reactor section.

In film theory, a diffusive transport within the boundary layer is assumed. Using this assumption, and considering the boundary layer thickness uniform along the biofilm, equation (3) (Reiss and Hanratty, 1963) has been typically used to estimate mass transfer coefficient from boundary layer thickness measurement using microsensors (Horn and Hempel, 1995; Wäsche et al., 2002; Zhang and Bishop, 1995).

$$k_L = \frac{D_i}{L_c} \qquad (3)$$

Where D_i is the effective diffusivity within the boundary layer ($m^2 \cdot s^{-1}$), and L_c is the boundary layer thickness (m). The main drawback of this approach is that the effect of boundary layer irregularities (caused by biofilm surface roughness (C. Picioreanu et al., 2000) on external mass transport is neglected.

2.3.2. Internal mass transport

Biofilms are commonly described as a heterogeneous phase comprising a matrix of bacteria and extracellular polymeric substances and a large amount of water within matrix voids (Hinson and Kocher, 1996). Consequently, solute transport within biofilms is the result of diffusion through the denser aggregates and convective transport through the pores and water channels (De Beer et al., 1994a; Horn and Morgenroth, 2006; Picioreanu et al., 2000). However, internal mass transport can be described considering biofilms as a homogeneous phase in which mass transport is driven by diffusion while including the influence of biofilm heterogeneity in the effective diffusivity (Stewart, 1998). Therefore, reliable estimates of effective effective

diffusivities within biofilms are required to ensure models consistency. In this work, mass transport was described using a non-steady-state diffusion model (Fick's second law) as shown in equation (4).

$$\frac{dC_{DO,b}}{dt} = D_b \frac{\partial^2 C_{DO,b}}{\partial z^2} \qquad (4)$$

Where $C_{DO,b}$ is the DO concentration inside the biofilm ($mg \cdot L^{-1}$), t is time (s), z is the biofilm depth (m), and D_b is the effective diffusivity within biofilms ($m^2 \cdot s^{-1}$), which depends on biofilm heterogeneity.

2.4. Mass transport coefficients estimation

The external mass transfer coefficient and effective diffusivities were estimated using an optimization procedure. The differential equations (1), (2) and (4) were solved using a variable step Runge-Kutta method and a numerical method for boundary value problems of ordinary differential equations, respectively. Parameters were estimated by curve-fitting of model estimates to experimental data using a Nelder-Mead simplex algorithm (unconstrained non-linear optimization). To this aim, the DO concentrations measured with microsensors and predicted by both equations were used to compute the objective function, as shown in equation (5).

$$F = \sqrt{\sum_{i=1}^{n} \left[y_{\exp,i} - y_{\theta,i} \right]} \qquad (5)$$

Where F is the objective function to minimize, n is the number of experimental measurements, $y_{\theta,i}$ is the simulated oxygen concentration ($mg \cdot L^{-1}$) and $y_{exp,i}$ is the experimentally measured oxygen concentration ($mg \cdot L^{-1}$). The described simulation and minimization procedures resulting in parameters optimization was carried out in Matlab R2013a.

2.4.1. Confidence Intervals

In the present study the confidence intervals of the estimated mass transport parameters were assessed through the Fisher Information Matrix (FIM) following the procedure described in Dorado et al., (2008), which is based on previous works (Guisasola et al., 2006). Considering white noise in DO measurements and a reliable model, the increase of the FIM provides the lower bound of the parameters estimation covariance matrix, which can be used to quantify the uncertainity of the optimized parameters.

2.4.2. Optimal experimental design for parameters estimation

Optimal experimental design (OED) was based on selecting the optimal experimental conditions to obtain an accurate estimation of model parameters. The influence of data obtained in these experiments on estimates accuracy was assessed.

According to experimental measurements available, DO at different locations along the reactor were selected as output variables. Therefore, the OED was reduced to study the effect on the estimates precision of the input variables (initial conditions) and the sampling conditions.

The variables considered in the OED for external mass transfer coefficients estimation were the DO concentration in the liquid phase at the inlet of the FPB ($C_{DO,L\ (inlet)}$), the initial DO concentration in the liquid boundary layer ($C_{DO,L\ (t=0)}$) and biofilm surface ($C_{DO,B\ (t=0)}$), the sampling frequency ($v_{sampling}$), the monitoring time (t_{exp}), and the interfacial area of the monitored system ($A_{transfer}$). On the other hand, the experimental variables selected in the OED to assess the effective diffusivity were $C_{DO,L\ (inlet)}$, $C_{DO,B\ (t=0)}$, $v_{sampling}$, t_{exp}, the depth along the DO profile ($z_{profile}$) and the distance between monitoring points ($\Delta z_{profile}$).

Equations (1) and (4) were used to obtain model estimations in a battery of experimental conditions according to Table 1. In this procedure, the FIM method was included in models to estimate the confidence intervals of mass transport parameters. The confidence intervals served to determine the uncertainty of model parameters by means of the uncertainty percentage (% uncertainty) calculated as the variation of the confidence intervals with respect to their central values.

311

312

313 **Table 1.** Variables scrutinized in the OED of both the external mass transfer coefficient and the
314 effective diffusivity.

	Studied variable	Initial value	End Value
k_L OED	$C_{DO,L\ (inlet)}$ [mg·L^{-1}]	6	8.5
	$C_{DO,L\ (t=0)}$ [mg·L^{-1}]	4	7
	$C_{DO,B\ (t=0)}$ [mg·L^{-1}]	1	4
	$A_{transfer}$ [m^2]	$2 \cdot 10^{-3}$	$7 \cdot 10^{-3}$
	$v_{sampling}$ [s^{-1}]	1	0.1
	t_{exp} [s]	200	500
D_b OED	$C_{DO,L\ (inlet)}$ [mg·L^{-1}]	4	8
	$C_{DO,B\ (t=0)}$ [mg·L^{-1}]	0	2.5
	$\Delta z_{profile}$ [µm]	25	100
	$Z_{profile}$ [cm]	0.1	0.2
	$v_{sampling}$ [s^{-1}]	1	0.1
	t_{exp} [s]	100	1800

315

316 ## 3. Results

317 ### 3.1 Optimal experiment design for parameter estimation

318 The OED to estimate model parameters was performed evaluating the estimation accuracy
319 under different experimental scenarios. Figure 3 shows the OED results for the external mass
320 transfer coefficient estimation. The evolution of parameters uncertainty is plotted against the
321 value of the selected variables. Results revealed that the control of the initial DO concentration
322 in the liquid interphase (figure 3b) and the transfer area (figure 3d) were not critical to reduce

results uncertainty. Results indicate that the accuracy on k_L estimation could be enhanced by stopping the deoxygenation when the DO concentration at the biofilm surface was below 2 $mg \cdot L^{-1}$ (figure 3c) and re-aerating until a DO concentration in the liquid phase above 6 $mg \cdot L^{-1}$ (figure 3a). These results also highlighted that oxygenation profiles should be recorded during at least 500 s (figure 3f) using a sampling frequency of 1 s^{-1} (figure 3e).

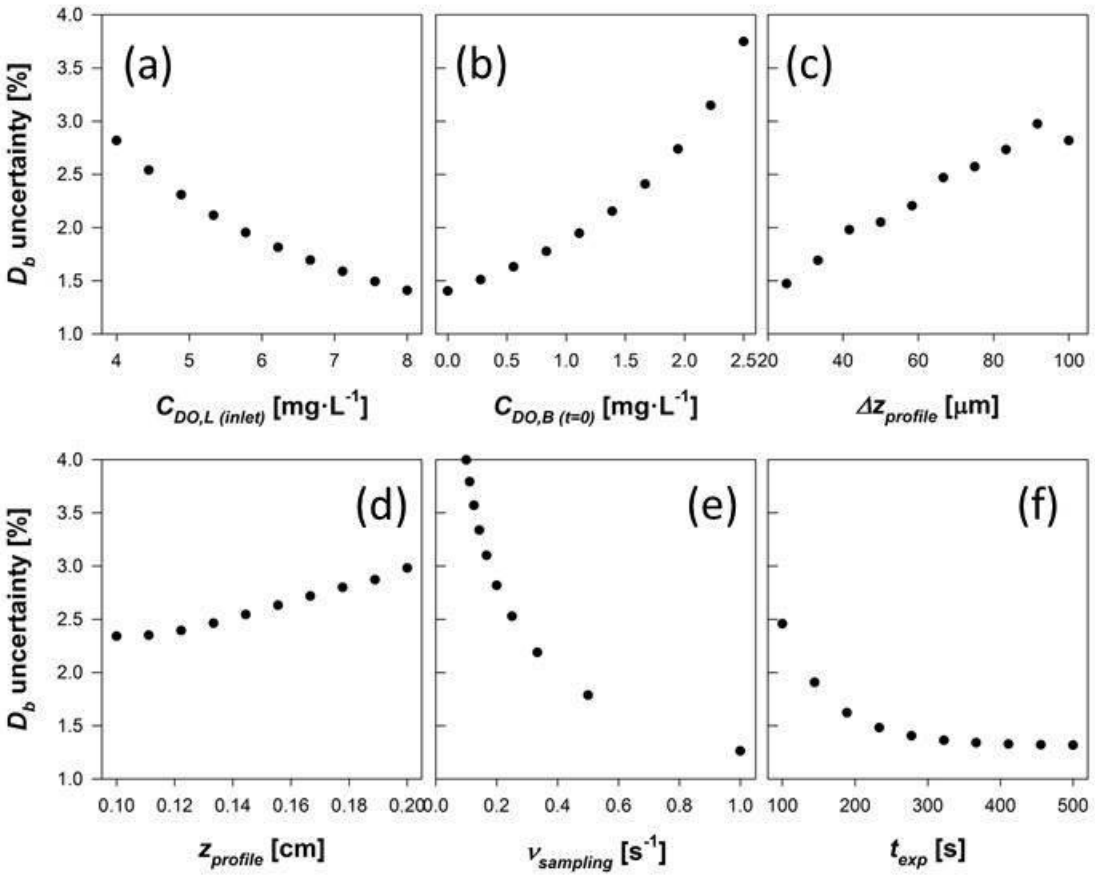

Figure 4. Uncertainty of effective diffusivity (D_b) against (a) the DO concentration at the inlet of the reactor; (b) the initial DO concentration at the biofilm surface; (c) the interval between monitored depths; (d) the monitored thickness of the biofilm; (e) the sampling frequency; and (f) the sampling time.

The experimental conditions under which internal mass transport coefficients were estimated were also assessed (figure 4). The OED results showed that the control of all selected input variables was critical for minimizing the uncertainty of resulting parameters in the estimation of the effective diffusivity. Thus, recording of oxygenation profiles started when the DO concentration on biofilm surface was below 2 $mg \cdot L^{-1}$ (figure 4b), and the system was

oxygenated until a DO concentration in the liquid phase above 7 $mg \cdot L^{-1}$ was reached (figure 4a). In addition, the resulting oxygenation profiles were recorded for at least 500 s (figure 3f) with a sampling frequency of 1 s^{-1} (figure 4e). Results (figure 4c and figure 4d) also allowed selecting the optimal sensor configuration from three available designs. The first design of the microsensor, allowing monitoring of 1 mm depth biofilm at 50 µm intervals, was selected. Additional information of the microsensor configuration can be found in table S1 (supplementary information).

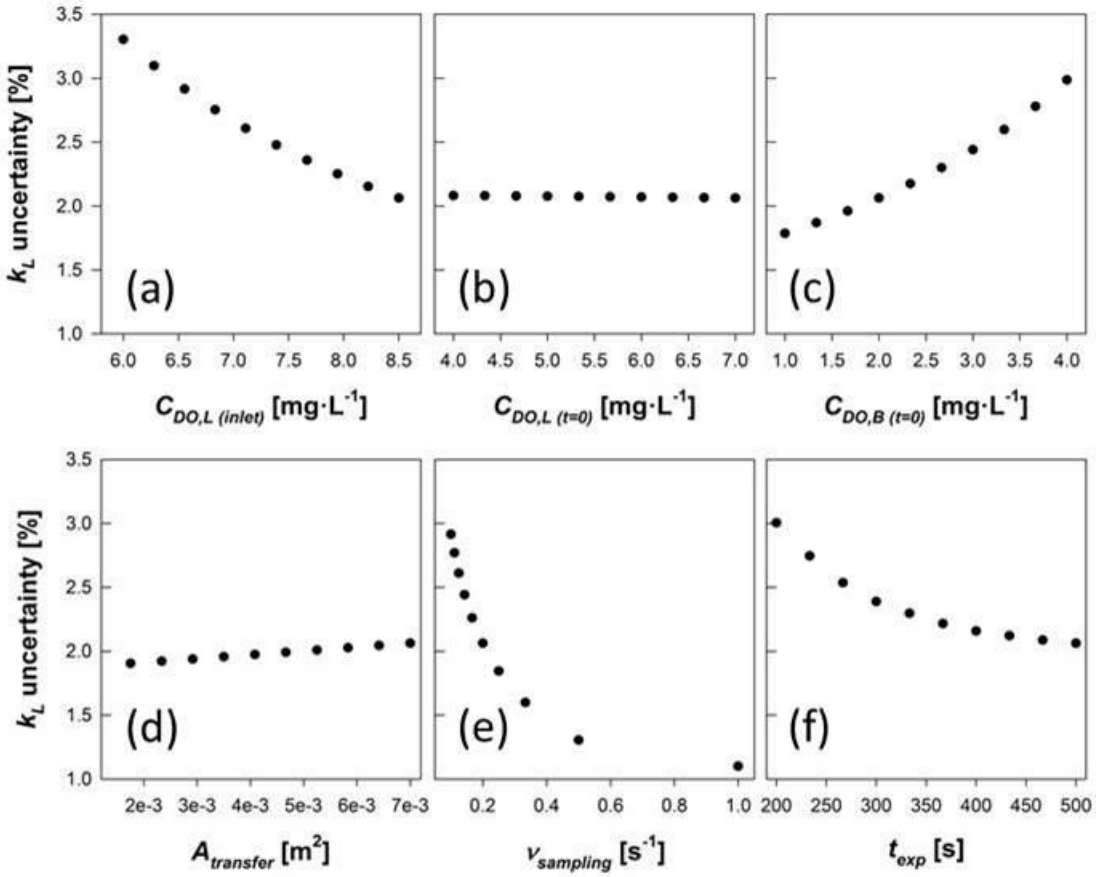

Figure 3. Uncertainty of external mass transport coefficient (k_L) against (a) DO concentration at the inlet of the reactor; (b) the initial DO of the recorded oxygenation profiles within the liquid interphase; (c) the intial DO concentration on the biofilm surface; (d) the interfacial area of monitored system; (e) the sampling frequency; and (f) the sampling time.

3.2 External mass transport characterization

Mass transport resistance in the liquid boundary layer was experimentally quantified considering boundary layer irregularities. With this aim, the oxygen flux towards the liquid-biofilm interphase was monitored by measuring oxygen profiles at both sides of the boundary layer (spatial resolution of 50 μm). The location of the sensors in the FPB was selected based on previous measurements that ensured accomplishing the OED criteria, and corresponded to the center of the open channel (reactor). Simulated and experimental oxygenation profiles located in the middle of the FPB are shown in figure 5a. Simulated profiles in the liquid boundary layer and on the biofilm surface showed a good agreement with recorded profiles, confirmed by the normalized root mean square error (NRMSE) (4.55% for DO profiles in the liquid boundary layer and 9.22% for DO profiles on biofilm surface). Results shown in figure 5a revealed a fast oxygenation of the liquid phase from the beginning of the recording period. The initial DO (7.6 $mg \cdot L^{-1}$) was close to saturation conditions and only increased 1 $mg \cdot L^{-1}$ during the overall period. On the other hand, the resistance to oxygen transport across the boundary layer clearly determined the oxygen concentration evolution at the biofilm surface. In this sense, the initial concentration at the boundary layer was 1.6 $mg \cdot L^{-1}$ while a slow but extensive oxygenation up to 7 $mg \cdot L^{-1}$ was observed. Each profile was used to estimate a single mass transfer coefficient towards the liquid interphase (k_L).

Influence of hydrodynamic conditions on the external mass transfer coefficient was assessed by repeating the procedure at liquid velocities between 2.5 $m \cdot h^{-1}$ and 25 $m \cdot h^{-1}$, which corresponded to a range of laminar Re numbers between 0.5 and 7 (figure 5b). Results show the effect of flow conditions on mass transfer resistance. As can be observed, mass transfer resistance between the liquid phase and the biofilm surface decreased with the increase of liquid velocity. This trend is in agreement with previous works (Horn and Hempel, 1997; Prades et al., 2015; Wäsche et al., 2002; Zhang and Bishop, 1995) that described a reduction of the thickness of the stagnant liquid layer at increasing liquid phase velocities (Zhang and Bishop, 1995). In consequence, mass transfer rate is enhanced.

Despite few authors (Picioreanu et al., 2000; Zhang and Bishop, 1995) focused their studies on experimental systems and operating conditions close to those used in the current work, results were compared with empirical and theoretical correlations in order to advance in the understanding of the mechanisms involved in mass transfer resistance between the fluid and the biofilm phases. In this regard, a careful comparison was required since it is known that mass transfer resistance depends on the hydrodynamics, the geometry of the enclosed conduit and the physical properties of the fluid. Experimental mass transfer coefficients found in literature are mainly calculated from L_c measurements only considering diffusion within the boundary layer. Zhang and Bishop (1995) results showed a good agreement with theoretical models developed using the Blasius solution under laminar flow conditions, equation (6), but provided poor estimates of experimental k_L as shown in figure 5b.

$$Sh = 0.369 \cdot \mathrm{Re}^{0.5} \cdot Sc^{0.33} \qquad (6)$$

Where *Sc* is the Schmidt number, related to the physical properties of the fluid. The deviation of the laminar trend described by equation (6) with respect to the experimental results revealed that a thorough analysis was required. Such discrepancy was explained by the effect of the biofilm surface roughness on mass transfer mechanisms. Some authors considered this surface effect (Beyenal and Lewandowski, 2000; C. Picioreanu et al., 2000; Wäsche et al., 2002), concluding that due to the combination of several mass transfer mechanisms within the boundary layer, the linear approach, shown in equation (3), is not close to reality. Therefore, laminar models considering a Blasius boundary layer presented some reliability problems to describe mass transfer through liquid-biofilm interphases. The dynamic oxygenation procedure used herein allowed including all mass transfer mechanisms in the external mass transfer coefficient. Data obtained herein was used to propose a Sh-Re correlation based, in equation (7), that provided a reliable, overall, mass transfer description (figure 5b). As reported in Picioreanu et al. (2000) the turbulences within the boundary layer resulted in the increase of the Re exponent, in this case close to those values found for turbulent models (Horn and Lackner, 2014).

395 $$Sh = 0.239 \cdot \mathrm{Re}^{0.8} \cdot Sc^{0.33} \qquad (7)$$

396 Physical properties of the fluid used in dimensionless numbers calculation describing equation
397 (6) and equation (7) are detailed in section S5 of Supplementary Material (Table S3).

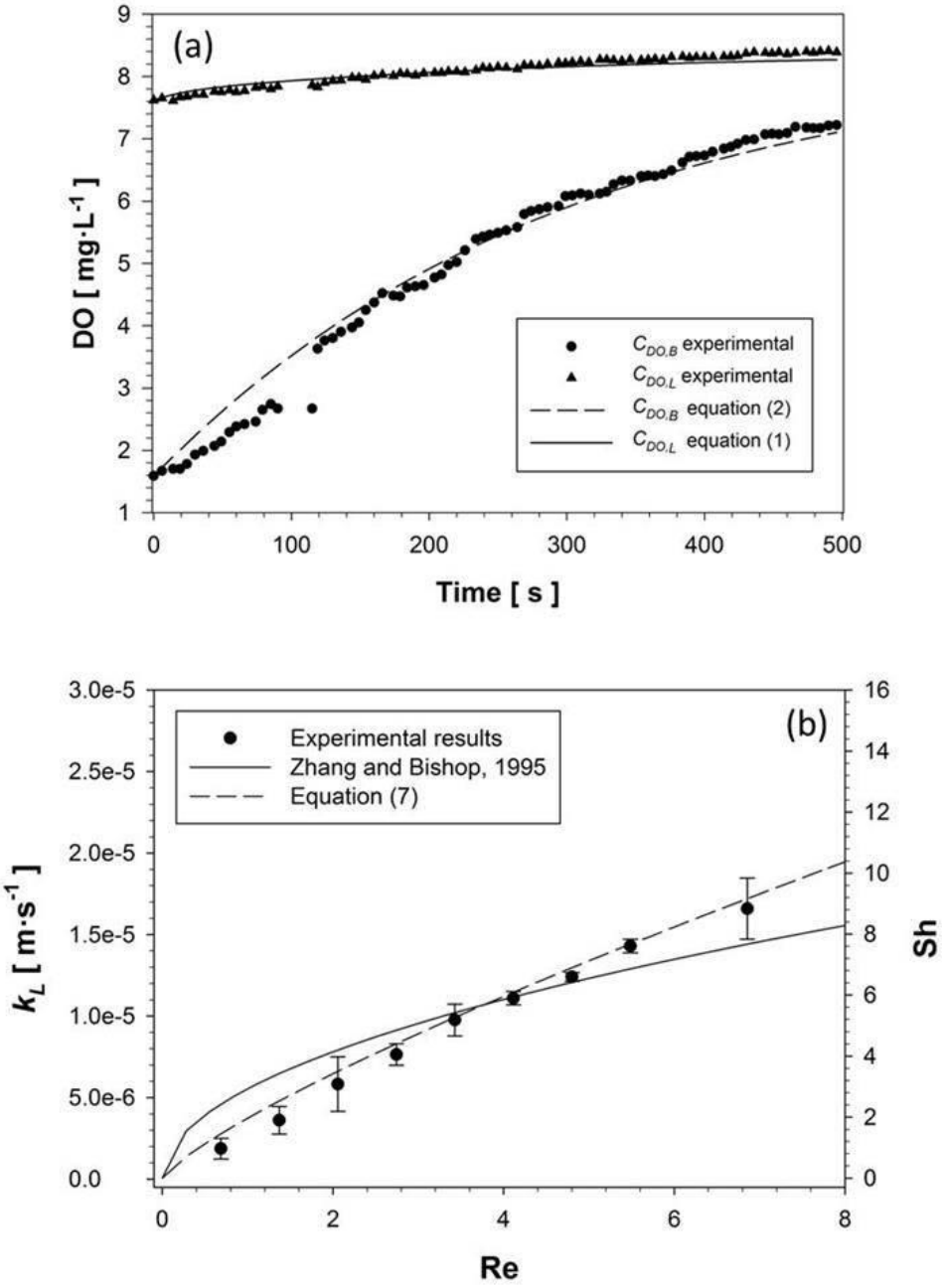

Figure 5. (a) Example of experimental and simulated DO concentration in the liquid boundary layer and at the biofilm surface. (b) Mass transfer coefficient, experimentally estimated herein and calculated using equation (5) and equation (6) are shown as absolute k_L and Sherwood number as a function of the Reynolds number.

398

3.3 Internal mass transport characterization

Internal mass transport was characterized within biofilms grown in the FPB by the simultaneous recording of dynamic oxygenation profiles at different depths inside biofilms using the DO-MEA microsensor. The location of the sensors in the FPB was also selected based on previous measurements (not shown) that ensured accomplishing the OED criteria Experimental DO profiles served to estimate an average effective diffusivity by curve-fitting of equation (4) to experimental data. Figure 6a shows the experimental and simulated (surface plot) profiles obtained in a biofilm section of a density of 21.20 g VSS·L^{-1} at a liquid flow velocity of 9.88 m·h^{-1}(Re 2.8).

Figure 6a reveals the DO distribution through the deactivated biofilm. At the beginning of the re-aeration phase, the DO concentration inside the biofilm decreased from 2.5 mg DO·L^{-1} at the biofilm surface to 1 mg·L^{-1} at a 700 μm depth. An almost homogeneous oxygenation rate of about $1.5 \cdot 10^{-3}$ mg·DO $L^{-1} \cdot s^{-1}$ (calculated from the slope of experimental oxygenation profiles) was observed within the entire biofilm during the monitoring period. At the end of this period, the oxygenation rate was reduced resulting in a smoother DO profile between the biofilm surface and the inner parts of the biofilm, where the DO concentration ranged from 4.5 mg·DO L^{-1} to 4 mg·DO L^{-1} as a result of mass transport resistance. Figure 6a also shows a good fitting between the experimental and simulated data (NRMSE of 8.43%) providing a reliable estimation of oxygen effective diffusivity. These coefficients were used to calculate the intrinsic diffusion within biofilms. To this aim, effective diffusivities were translated to a dimensionless form (D_r) using the molecular oxygen diffusion (D_w) (Nguyen et al., 2014) as described in Beyenal and Lewandowski (2000).

Since a reliable mass transport approach depends on the quality of effective diffusivities, the biofilm heterogeneity effect should be considered. Thus, the effective diffusivity was quantified considering the influence of both hydrodynamic conditions and biofilm density according to the impact of the structural heterogeneity in the assessment of internal mass transport mechanisms

425 within biofilms previously described through biofilm density data (Bishop et al., 1995; De Beer
426 et al., 1994b; Melo and Frias, 2004) and through hydrodynamic data (De Beer et al., 1996,
427 1994a; Stoodley et al., 1997).

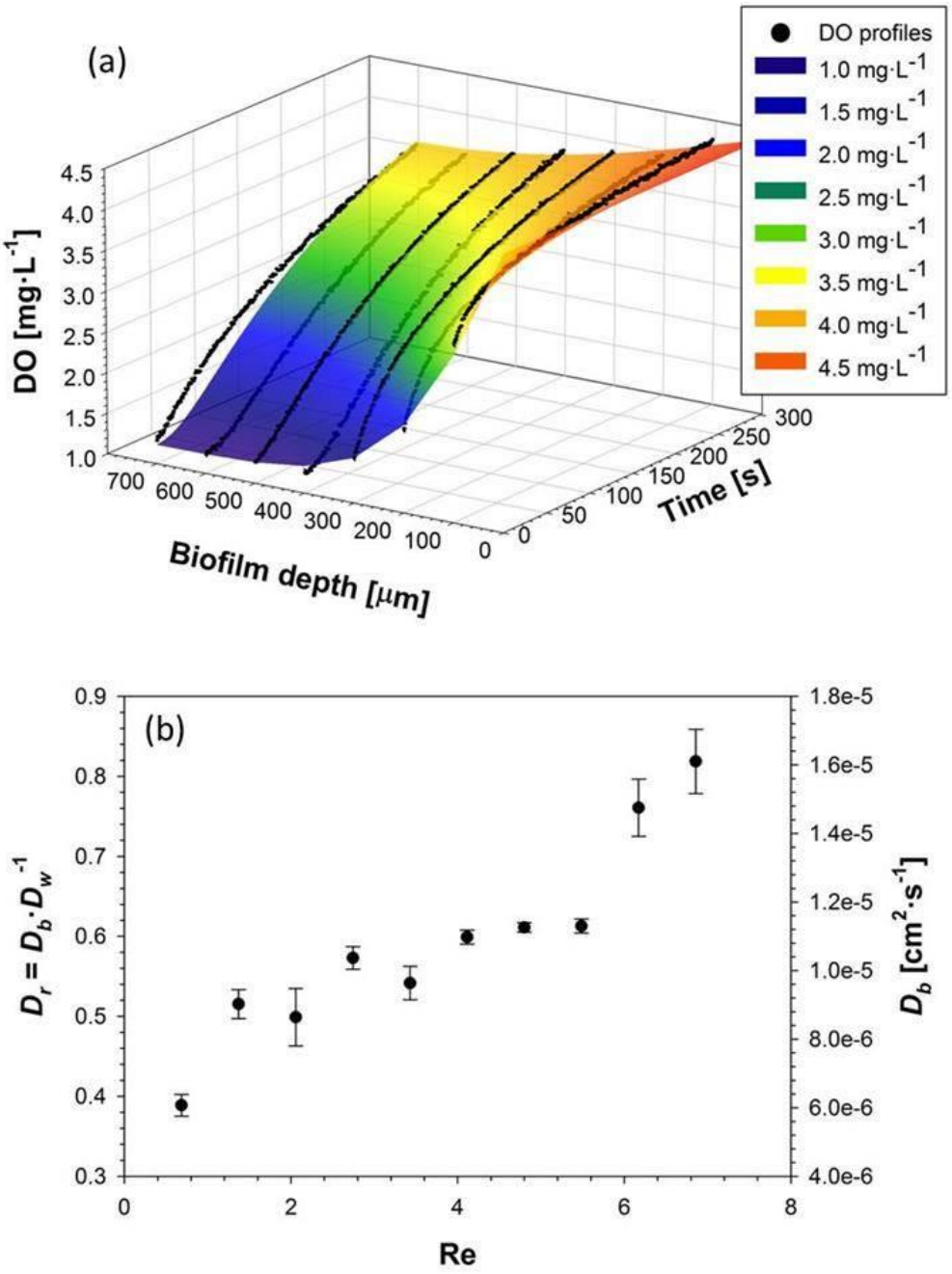

Figure 6. (a) Simulated (surface plot) and experimental (●) dynamic dissolved oxigen profiles obtained in a single-shot, 6-points measurement used in the determination of oxygen effective diffusivity of a biofilm section. (b) Experimental average (D_b) and dimensionless (D_r) oxygen effective diffusivity (●) in a biofilm section of 21.20 g VSS·L^{-1} estimated at different liquid flow velocities.

428

429 *3.3.1 Effect of hydrodynamic conditions on effective diffusivity determination*

Since the evaluation of hydrodynamic conditions inside biofilms, which are often described as a static phase, is complex and requires additional and sophisticated equipment (Stoodley et al., 1994), local effective diffusivities were characterized considering the convective contribution on mass transport within the biofilm. Thus, different hydrodynamic conditions in the liquid phase were set by changing the liquid velocity. In figure 6b, the effective diffusivities estimated at different liquid velocities within a biofilm section of 21.20 g $VSS \cdot L^{-1}$, are shown. At Re below 2.8 the oxygen diffusion decreased from 60% to 40% of its value in water. Estimated effective diffusivities were almost constant ($1.1 \cdot 10^{-5}$ $cm^2 \cdot s^{-1}$) at Re between 2.8 and 5.6, while higher effective diffusivities, even close to oxygen diffusion in water were observed at Re above 5.6. The three different behaviors observed were related to the biofilm heterogeneity and mass transport mechanisms taking place. Stoodley et al. (1997) observed no changes in the local mass transfer coefficient in the liquid channels at low liquid velocities. In our case we observed that below 10 $m \cdot h^{-1}$ (Re 2.8) mass transport inside biofilms was controlled by diffusion leading to lower effective diffusivities. On the other hand, De Beer et al. (1996) found that over a critical liquid velocity mass transport through the voids became increasingly significant and that convection within liquid voids and channels enhanced mass transport of substrates through biofilms. Due to this phenomenon, at Re above 5.6, mass transport in biofilms was driven by convection with effective diffusivities close to convective coefficients. Between Re 2.8 and 5.6 mass transport was the result of combining convective and diffusive mechanisms and a steady trend of the effective diffusivity along the velocity range was observed.

3.3.2 Influence of biofilm density on effective diffusivity determination

Biofilm heterogeneity has been commonly considered as the link between biofilm structure and mass transport rates. In the current work, an increasing of biofilm density from the inlet to the outlet of the FPB was observed. The density profile between 9 g $VSS \cdot L^{-1}$ and 70 g $VSS \cdot L^{-1}$ (corresponding with biofilm porosities between 0.96 and 0.72) was used to experimentally correlate effective diffusivity with biofilm density. With this aim, the dynamic oxygenation procedure was applied at different locations along the reactor, measuring biofilm density at each

457 monitored point. According to figure 6b, the liquid phase velocity was set at 10 $m \cdot h^{-1}$ (Re 2.8)
458 in all measurements to ensure that the oxygen effective diffusivity was not influenced by the
459 liquid flow velocity. Figure 7a shows the effective diffusivities estimated as a function of the
460 biofilm density.

461 Results in figure 7a show a linear decrease of the effective diffusivity from the 80% to the 32%
462 when the biofilm density increased from 9 to 33 g $VSS \cdot L^{-1}$. Results also showed that mass
463 transport was strongly limited within biofilms of densities above 50 g $VSS \cdot L^{-1}$ with estimated
464 diffusion rates about the 5% of their value in water. This trend is explained because a higher
465 biofilm density resulted in a decrease of biofilm porosity and, thus, less open volume was
466 available for the diffusion of oxygen through the biofilm.

467 Several works have developed diffusion models considering the influence of biofilm
468 heterogeneity, commonly addressed from a structural parameter. These models are shown in
469 detail in section S4 of Supplementary Material. However, authors warned about reliability
470 problems, limiting the use of these correlations in different experimental systems. In the current
471 work, a comprehensive analysis of diffusion models was performed comparing the results found
472 herein with the most relevant diffusion correlations (figure 7a). Correlations tested were adapted
473 to estimate the dimensionless effective diffusivity from biofilm density. Experimental results
474 were in agreement with most of the theoretical and experimental correlations found in literature
475 (Beyenal et al., 1997; Fan et al., 1990; Hinson and Kocher, 1996; Horn and Morgenroth, 2006;
476 Zhang and Bishop, 1994) at biofilm densities below 40 g $VSS \cdot L^{-1}$. However, in denser biofilms
477 only experimental correlations (Horn and Morgenroth, 2006) showed diffusivities close to those
478 experimentally estimated herein. Theoretical correlations predicted a slower decrease of
479 effective diffusivity when biofilm density increases, showing relative effective diffusivities
480 about 0.2 within biofilms denser than 100 g $VSS \cdot L^{-1}$.

481 The largest deviations were observed with respect to the Zhang and Bishop (1994) equation,
482 constructed from a porous catalyst model considering biofilms as a porous matrix within of

483 which diffusion drives mass transport; and also with respect to the Beyenal et al. (1997)
484 equation, developed by extrapolating estimated diffusivities from flocculent biomass densities
485 between 40 g $VSS \cdot L^{-1}$ and 100 g $VSS \cdot L^{-1}$ to the entire biomass density range. Similarly, the Fan
486 et al. (1990) equation overestimated the experimentally observed diffusivities. Such behavior
487 was explained because this correlation was developed considering effective diffusivities
488 estimated within biomass flocs in the higher density range. Therefore, this correlation showed
489 some reliability problems describing biofilms internal mass transport. The Hinson and Kocher
490 (1996) equation showed the same trend observed in the results of the Fan model since the
491 former model was developed correcting the Fan correlation with experimental results in
492 biofilms of densities below 60 g $VSS \cdot L^{-1}$. On the other hand, the Horn and Morgenroth (2006)
493 equation, that was developed from experimental effective diffusivity estimates within biofilms,
494 fitted well the experimental results both for high and low biofilm densities. The largest
495 differences were observed at lower densities, where the correlation overestimated the biofilm
496 effective diffusivity with values even higher than in water. As explained by the authors, this
497 deviation was caused by the large scatter of data used in the development of their correlation.

498 The above comparison of results of experimental diffusivities and diffusivities predicted by
499 correlations highlighted the difficulty of using correlations to describe mass transport in a
500 different system. Therefore, extrapolation and usage of literature data should be made carefully.
501 Results presented herein showed that development of internal mass transport correlations from a
502 thorough experimental study performed on the modeled system is recommended. For this
503 reason, the methodology developed herein to quantify effective diffusivity could be a powerful
504 tool since allows an easy characterization under a wide range of conditions.

505 ### *3.3.3 Proposed empirical correlation for biofilm effective diffusivity*

506 Experimental data and estimated effective diffusivity obtained using the methodology based on
507 dynamic dissolved oxygen profiles assessed under a wide range of conditions was used to
508 propose an experimental correlation for the effective diffusivity, depicted in figure 7b.

509 Considering that the oxygen diffusion within biofilms showed a clear dependence on the biofilm
510 density and the hydrodynamic conditions, a simple diffusion model was developed correlating
511 experimental results presented in figure 6b and figure 7a. Experimental data was fitted using
512 Minitab software with a general multi-variable model. The resulting correlation, equation (8),
513 allowed the calculation of the dimensionless effective diffusivity as a function of the biofilm
514 density and the Re in the open channel.

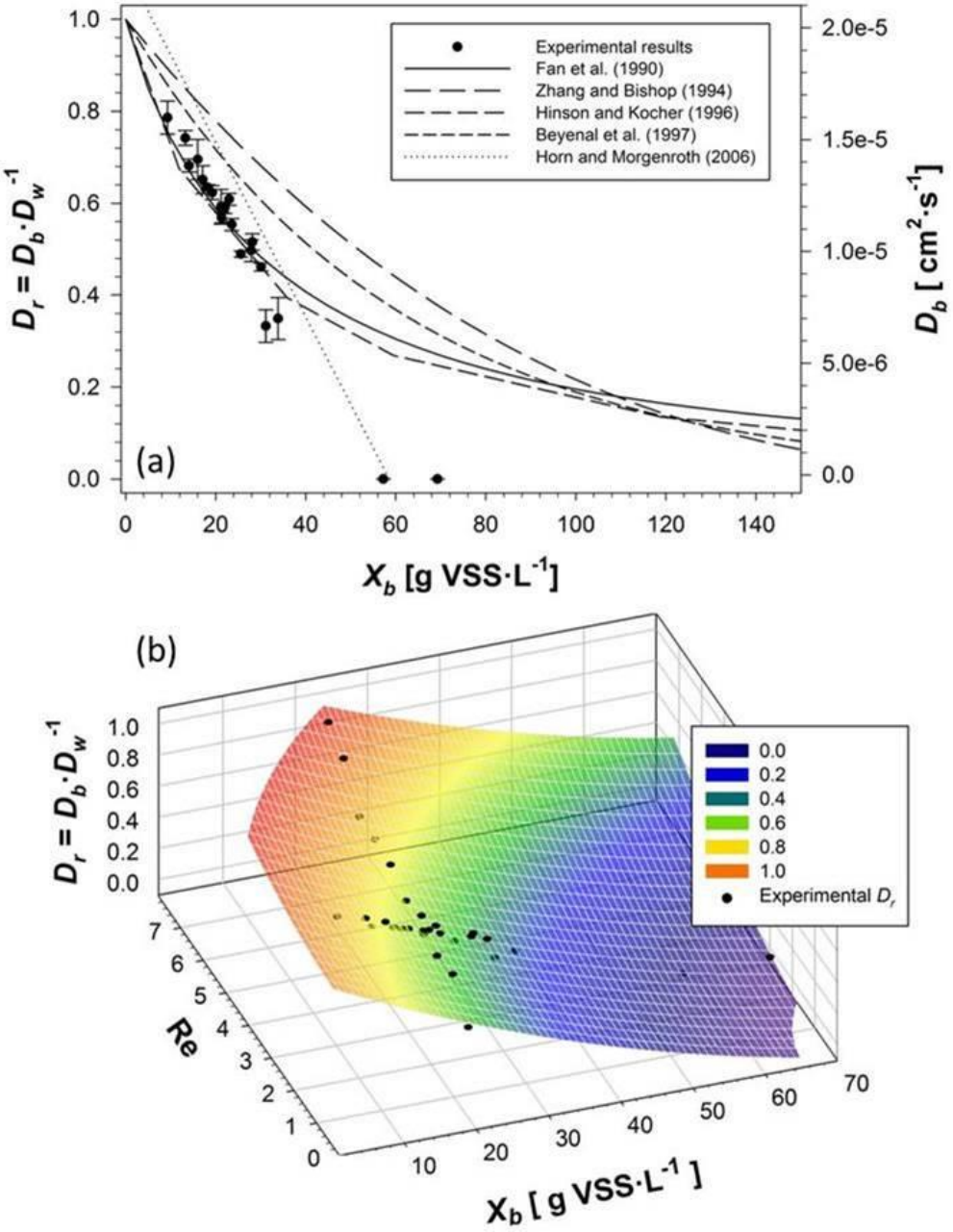

Figure 7. (a) Experimental (●) and theoretical average oxygen effective diffusivity (D_b) and dimensionless effective diffusivity (D_r) at a flow velocity of 9.88 m·h^{-1} as a function of the biofilm density. (b) Dimensionless effective diffusivity predicted by a general multi-variable model (surface plot) and estimated experimentally (●) at different liquid phase velocities and biofilm densities.

$$D_r = 0.93 - 0.023 \cdot X_b + 1.17 \cdot 10^{-2} \cdot \mathrm{Re}^2 + 1.1 \cdot 10^{-4} \cdot X_b^2 \qquad (8)$$

Where D_r is the dimensionless effective diffusivity, X_b is the biofilm density (g VSS·L^{-1}) and Re is the Reynolds number in the open channel. The good agreement, observed in figure 7b

519 between the surface of effective diffusivities predicted by equation (8) and the experimentally
520 estimated effective diffusivities was confirmed by the correlation factor (0.949).

521 ## 4. Conclusions

522 Microsensors measurements and the use of a dynamic monitoring of DO through the re-aeration
523 method have proven to be an excellent tool for internal and external mass transport
524 characterization. To the best of our knowledge this is the first time that both mass transport
525 mechanisms have been completely characterized using microsensors and the re-aireation
526 method. In addition, an OED improves the accuracy on the estimation of mass transport
527 parameters. Results obtained within heterotrophic biofilms have confirmed that, due to surface
528 roughness influence, the Blasius solution is not suitable for fluid-biofilm mass transfer
529 description. Regarding to internal mass transport, results obtained suggested that this
530 phenomenon is driven by a combination of convective and diffusive mechanisms. For this
531 reason, it is recommended to use diffusion models considering both hydrodynamic conditions
532 and biofilm density. On the other hand, the comparison of experimental results with mass
533 transport correlations highlighted the need of experimental measurements to describe mass
534 transport in biofilms rather than the available correlations. Overall, this research shows the
535 benefit of using microsensor-based measurements to provide high-quality information for
536 external and internal mass transport resistances characterization within biofilms, which is
537 essential to improve the performance of biofilm-based reactors. In addition, results obtained
538 using these methodologies provided fundamental background clarifying mass transport
539 mechanisms involved in biofilms systems.

540 **Acknowledgements**

541 This work has been founded by the project CTM2012-37927-C03-02, financed by the
542 Ministerio de Economía y Competitividad (Spain). Xavier Guimerà acknowledges a FPI-UPC
543 predoctoral scholarship, from Universitat Politècnica de Catalunya. The authors also want to
544 acknowledge the Biomedical Applications Group (GAB), and especially to Ana Moya, from the

Barcelona Microelectronics Institute (IMB-CNM, CSIC) their work in the DO-MEA sensor development.

References

Beuling, E.E., van Den Heuvel, J.C., Ottengraf, S.P., 1999. Diffusion coefficients of metabolites in active biofilms. Biotechnol. Bioeng. 67, 53–60.

Beyenal, H., Lewandowski, Z., 2005. Modeling mass transport and microbial activity in stratified biofilms. Chem. Eng. Sci. 60, 4337–4348. doi:10.1016/j.ces.2005.02.063

Beyenal, H., Lewandowski, Z., 2000. Combined effect of substrate concentration and flow velocity on effective diffusivity in biofilms. Water Res. 34, 528–538.

Beyenal, H., Seker, S., Tanyolaç, A., 1997. Diffusion Coefficients of Phenol and Oxygen in a Biofilm of Pseudomonas putida. AIChE J. 43, 243–250.

Bishop, P.L., Zhang, T.C., Fu, Y.-C., 1995. Effects of biofilm structure, microbial distributions and mass transport on biodegradation processes. Water Sci. Technol. 31, 143–152.

Bonilla-Blancas, W., Mora, M., Revah, S., Baeza, J.A., Lafuente, J., Gamisans, X., Gabriel, D., González-Sánchez, A., 2015. Application of a novel respirometric methodology to characterize mass transfer and activity of H2S-oxidizing biofilms in biotrickling filter beds. Biochem. Eng. J. 99, 24–34.

Bradford, M.M., 1976. A rapid and sensitive method for the quantitation of microgram quantities of protein utilizing the principle of protein-dye binding. Anal. Biochem. 72, 248–254.

De Beer, D., Stoodley, P., Lewandowski, Z., 1996. Liquid flow and mass transport in heterogeneous biofilms. Water Res. 30, 2761–2765.

De Beer, D., Stoodley, P., Lewandowski, Z., 1994a. Liquid flow in heterogeneous biofilms. Biotechnol. Bioeng. 44, 636–641.

De Beer, D., Stoodley, P., Roe, F., Lewandowski, Z., 1994b. Effects of biofilm structures on oxygen distribution and mass transport. Biotechnol. Bioeng. 43, 1131–1138.

Devinny, J.S., Deshusses, M.A., Webster, T.S., 1999. Biofiltration for air pollution control. Boca Raton, FL.

Dochain, D., Vanrolleghem, P.A., 2001. Dynamical Modelling and Estimation in Wastewater Treatment Processes. IWA Publishing, London.

Dorado, A.D., Baeza, J. a., Lafuente, J., Gabriel, D., Gamisans, X., 2012. Biomass accumulation in a biofilter treating toluene at high loads – Part 1: Experimental performance from inoculation to clogging. Chem. Eng. J. 209, 661–669.

Dorado, A.D., Baquerizo, G., Maestre, J.P., Gamisans, X., Gabriel, D., Lafuente, J., 2008. Modeling of a bacterial and fungal biofilter applied to toluene abatement: Kinetic parameters estimation and model validation. Chem. Eng. J. 140, 52–61.

Fan, L.-S., Leyva-Ramos, R., Wisecarver, K.D., Zehner, B.J., 1990. Diffusion of Phenol through a Biofilm Grown on Activated Carbon Particles in a Bioreactor. Biotechnol. Bioeng. 35, 279–286.

Fu, Y.C., Zhang, T.C., Bishop, P.L., 1994. Determination of effective oxygen diffusivity in biofilms grown in a completely mixed biodrum reactor, in: Water Science and Technology. pp. 455–462.

Guerrero, J., Guisasola, A., Baeza, J. a., 2011. The nature of the carbon source rules the competition between PAO and denitrifiers in systems for simultaneous biological nitrogen

589 and phosphorus removal. Water Res. 45, 4793–4802.
590 Guimerà, X., Moya, A., Dorado, A.D., Villa, R., Gabriel, D., Gabriel, G., Gamisans, X., 2014.
591 Biofilm dynamics characterization using a novel DO-MEA sensor: mass transport and
592 biokinetics. Appl. Microbiol. Biotechnol. 99, 55–66.
593 Hille, A., Neu, T.R., Hempel, D.C., Horn, H., 2009. Effective diffusivities and mass fluxes in
594 fungal biopellets. Biotechnol. Bioeng. 103, 1202–13.
595 Hinson, R.K., Kocher, W.M., 1996. Model for effective diffusivities in aerobic biofilms. J.
596 Environ. Eng. 122, 1023–1030.
597 Horn, H., Hempel, D.C., 1997. Substrate utilization and mass transfer in an autotrophic biofilm
598 system: Experimental results and numerical simulation. Biotechnol. Bioeng. 53, 363–71.
599 Horn, H., Hempel, D.C., 1995. Mass transfer coefficients for an autotrophic and a heterotrophic
600 biofilm system. Water Sci. Technol. 32, 199–204.
601 Horn, H., Lackner, S., 2014. Modeling of Biofilm Systems: A Review. Adv Biochem Eng
602 Biotechnol 146, 53–76.
603 Horn, H., Morgenroth, E., 2006. Transport of oxygen, sodium chloride, and sodium nitrate in
604 biofilms. Chem. Eng. Sci. 61, 1347–1356.
605 Mannucci, A., Munz, G., Mori, G., Lubello, C., 2012. Biomass accumulation modelling in a
606 highly loaded biotrickling filter for hydrogen sulphide removal. Chemosphere 88, 712–
607 717.
608 Melo, L.F., Frias, R.R., 2004. Biofilm physical structure , internal diffusivity and tortuosity.
609 Water Sci. Technol. 52, 77–84.
610 Moya, A., Guimerà, X., del Campo, F.J., Prats-Alfonso, E., Dorado, A.D., Baeza, M., Villa, R.,
611 Gabriel, D., Gamisans, X., Gabriel, G., 2014. Biofilm oxygen profiling using individually
612 addressable disk microelectrodes on a microfabricated needle. Microchim. Acta 182, 985–
613 993.
614 Nguyen, M.T., Appan, A., Tan, D.S., Tan, S.K., 2014. Influence of Small Water Surface
615 Perturbations on the Reaeration Process. J. Environ. Eng. 140, 1–7.
616 Ning, Y.-F., Chen, Y.-P., Li, S., Guo, J.-S., Gao, X., Fang, F., Shen, Y., Zhang, K., 2012.
617 Development of an in situ dissolved oxygen measurement system and calculation of its
618 effective diffusion coefficient in a biofilm. Anal. Methods 4, 2242.
619 Picioreanu, C., van Loosdrecht, M.C.M., Heijnen, J.J., 2000. A theoretical study on the effect of
620 surface roughness on mass transport and transformation in biofilms. Biotechnol. Bioeng.
621 68, 355–369.
622 Picioreanu, C., van Loosdrecht, M.C.M., Heijnen, J.J., 2000. Effect of diffusive and convective
623 substrate transport on biofilm structure formation: A two-dimensional modeling study.
624 Biotechnol. Bioeng. 69, 504–514.
625 Prades, L., Guimerà, X., Climent, J., Chiva, S., Dorado, A.D., Gamisans, X., 2015. Coupling
626 Hydrodynamics and Biodegradation Kinetics to Model Gas-Phase Biofiltration, in:
627 Biotechniques for Air Pollution Control 2015.
628 Reiss, L.P., Hanratty, T.J., 1963. An experimental study of the unsteady nature of the viscous
629 sublayer. AIChE J. 9, 154–160.
630 Stewart, P.S., 2003. Diffusion in Biofilms. J. Bacteriol. 185, 1485–1491.
631 Stewart, P.S., 1998. A review of experimental measurements of effective diffusive
632 permeabilities and effective diffusion coefficients in biofims. Biotechnol. Bioeng. 59,
633 261–272.
634 Stoodley, P., Lewandowski, Z., de Beer, D., 1994. Liquid Flow in Biofilm Systems. Appl.
635 Environ. Microbiol. 60, 2711–2716.

636 Stoodley, P., Yang, S., Lappin-scott, H., Lewandowski, Z., 1997. Relationship between mass
637 transfer coefficient and liquid flow velocity in heterogenous biofilms using
638 microelectrodes and confocal microscopy. Biotechnol. Bioeng. 50, 681–688.

639 Wäsche, S., Horn, H., Hempel, D.C., 2002. Influence of growth conditions on biofilm
640 development and mass transfer at the bulk/biofilm interface. Water Res. 36, 4775–84.

641 Yurt, N., Beyenal, H., Sears, J., Lewandowski, Z., 2003. Quantifying selected growth
642 parameters of Leptothrix discophora SP-6 in biofilms from oxygen concentration profiles.
643 Chem. Eng. Sci. 58, 4557–4566.

644 Zhang, T.C., Bishop, P.L., 1995. Experimental determination of the dissolved oxygen boundary
645 layer and mass transfer resistance near the fluid-biofilm interface. Water Sci. Technol. 30,
646 47–58.

647 Zhang, T.C., Bishop, P.L., 1994. Evaluation of tortuosity factors and effective diffusivities in
648 biofilms. Water Res. 28, 2279–2287.

649